Journal of Physics B: Atomic, Molecular and Optical Physics

On O(^{1}S) and CO(a ^{3} Pi) production from electron impact dissociation of CO_2

J. Phys. B: At. Mol. Opt. Phys. 27 (1994) 4039–4055. Printed in the UK

On $O(^1S)$ and $CO(a\ ^3\Pi)$ production from electron impact dissociation of CO_2

Lance R LeClair and J William McConkey

Department of Physics, University of Windsor, Windsor, Ontario, Canada N9B 3P4

Received 15 April 1994, in final form 17 June 1994

Abstract. A novel method is employed to selectively detect $O(^1S)$ and $CO(a\ ^3\Pi)$ fragments following the dissociation of CO_2 by electron impact. $O(^1S)$ atoms impinging on solid Xe produce a prominent emission feature at 725 nm, and less intense features at 375 and 550 nm. $CO(a\ ^3\Pi)$ molecules give a single emission feature spanning 250 to 350 nm. Time-of-flight spectra are presented for $O(^1S)$ and $CO(a\ ^3\Pi)$ from electron impact dissociation of CO_2. The results for $O(^1S)$ production indicate contributions from pre-dissociation of excited states of CO_2. Relative cross sections for the production of both species have been obtained. The cross section for $O(^1S)$ production has been made absolute by comparison with production of the same species from N_2O. It has a threshold at 11.0 ± 0.5 eV and reaches a maximum of 1.69×10^{-17} cm^2 at 50 eV.

1. Introduction

Electron impact dissociation (EID) of CO_2 has been a subject of study for the last 25 years. This has been due in large part to the observations of emissions from excited states of fragments in the airglows of Venus and Mars which arise partly from EID of CO_2 (e.g. Conway 1981, Fox and Dalgarno 1981). Knowledge of the integral cross section for various dissociation channels is important to the modelling of the upper atmospheres of those planets in order to determine sources of airglow and neutral particle heating (Fox and Dalgarno 1979). The neutral metastable fragments $O(^5S)$ and $CO(a\ ^3\Pi)$ have been observed directly following electron impact on CO_2 using either time-of-flight (TOF) spectroscopy (Barnett *et al* 1992 and references therein) or by observation of the fluorescence from $CO(a\ ^3\Pi)$ (Erdman and Zipf 1983). In the latter case, the absolute cross section for $CO(a\ ^3\Pi)$ production was measured to be 2.4×10^{-16} cm^2 at 80 eV.

Another significant cross section is one which results in the dissociation of CO_2 to produce $O(^1S)$ fragments. Strickland and Green (1969) have calculated a cross section for the $O(^1S)$ production channel

$$e + CO_2(X\ ^1\Sigma_g^+) \rightarrow e' + CO_2(1\ ^1\Sigma_u^+) \rightarrow CO(^1\Sigma^+) + O(^1S_0). \qquad (1)$$

Their calculation was based on the Bethe-Born approximation using an oscillator strength measurement for the $X\ ^1\Sigma_g^+ \rightarrow 1\ ^1\Sigma_u^+$ transition derived from electron energy loss spectroscopy (EELS). It was already known at the time that the $1\ ^1\Sigma_u^+$ state dissociates to $O(^1S)$ and $CO(X\ ^1\Sigma^+)$. The cross section reached a maximum of about

0953-4075/94/174039+17$19.50

$1.2 \times 10^{-17}\,cm^{-2}$ at 60 eV. A direct observation of all O(^{1}S) production from EID of CO_2 would enable an assessment of the contributions of other channels to (1).

Recently, the potential energy surfaces of excited states of CO_2 have been the subject of accurate *ab initio* calculations (Spielfiedel *et al* 1993 and references therein). The application of TOF spectroscopy to observe the production of O(^{1}S) metastable fragments following EID of CO_2 would be useful for comparison purposes.

Normally, O(^{1}S) is difficult to observe in experiments because of its long lifetime (0.8 s, Itikawa and Ichimura 1990). This makes it impossible in a normal laboratory situation to observe emission from O(^{1}S) (which decays predominantly to O(^{1}D) via the 5577 Å auroral line) because the atoms simply move out of the field of view before they radiate. Some methods have been devised to solve this problem, but all have significant shortcomings as discussed by LeClair and McConkey (1993).

In that paper, we reported absolute cross sections for O(^{1}S) production following EID of N_2O and O_2. This was made possible by the use of a detector made from solid Xe. O(^{1}S) atoms impinging on the layer of Xe produce XeO* emissions within several microseconds. The emission has a characteristic spectrum, with a dominant broad band at 725 nm, a weaker band at 375 nm and a much weaker band at 550 nm. We also demonstrated that the emissions from the Xe layer were solely due to the arrival of O(^{1}S) atoms. No emissions were observed following the arrival of other possible metastable fragments that could be produced by EID of O_2 and N_2O (such as O(^{1}D), $N_2(A\,^3\Sigma_u^+)$, or $O_2(a\,^1\Delta_g)$).

However, when studying O(^{1}S) production from CO_2, we find that in addition to the usual emission spectrum of O(^{1}S) from the Xe layer, there is a new feature at longer flight times with a broad emission band in the UV below 350 nm. Comparison of our time-of-flight spectra and excitation functions with earlier work lead us to identify this fragment as $CO(a\,^3\Pi)$. As far as we know, this if the first report on the use of solid Xe to detect $CO(a\,^3\Pi)$ in this manner.

2. Method and apparatus

To apply TOF spectroscopy to the production of neutral metastable particles following EID of a target molecule, a pulsed electron beam is directed through a target gas beam. At a distance d from the collision volume formed by the crossed beams a suitable detector is placed to record the arrival of metastable particles arising from electron impact on the target gas. The distribution of arrival times for the particles is denoted by $f(t)$. Changing the time-of-flight scale to a kinetic energy scale T is done using the expression $T = \frac{1}{2}m(d/t)^2$, where m is the mass of the detected fragment. Then $f(t)$ can be readily converted to a kinetic energy distribution $F(T)$ by the formula $F(T) \propto t^3 f(t)$.

If the detected metastable particles are the target molecule itself (i.e. no dissociation has occurred) then $f(t)$ is a Maxwell–Boltzman distribution. If the target gas dissociates into only two fragments, then, using conservation of momentum, the total released kinetic energy R is given by $R = T(M/m')$ where M denotes the total mass of the target molecule, and m' the mass of the undetected fragment. If the target molecule is diatomic, then the released kinetic energy distribution $F(R) \propto t^3 f(t)$ can be thought of as the reflection of the ground state wavefunction in the portion of the repulsive curve of the dissociating state which lies in the Franck–Condon region. Thus it is possible to use TOF spectra to determine the location of repulsive molecular curves in the FC region. If the target molecule is polyatomic, then it is difficult to get information about the

repulsive surface since the energy released from dissociation can go into vibrational and rotational modes of the fragment molecules.

There are several sources of systematic error associated with the actual application of TOF spectroscopy. These arise from the finite electron pulse width, size of the collision volume and detection region, response time of the detector, thermal spread of the target molecules, recoil of the parent molecule from electron impact, dependence of detection efficiency with particle velocity, and in-flight radiative decay of the metastable particle. These effects have been discussed previously (e.g. see Zipf 1984).

The apparatus used in these studies has been described in our previous paper (LeClair and McConkey 1993) so only a brief summary is presented here. It is a crossed beam apparatus in which the electron beam, target gas beam, and detector are mutually orthogonal. The electron gun is a high current magnetically collimated device which is differentially pumped. A capillary tube, 0.66 mm in diameter by 23 mm in length, forms the target gas jet. The driving pressure upstream of the capillary was typically 5 to 10 torr, as measured with a capacitance manometer. Deflection plates between the detector and collision region prevent unwanted ions and electrons from reaching the detector, and can be used to quench high lying ($n \gtrsim 20$) Rydberg fragments. No evidence of any contribution to our data from Rydberg fragments was observed.

The detector is a layer of solid xenon oriented at 45° to the incoming metastable fragments, placed in a differentially pumped chamber. This arrangement results in a TOF path of $d = 26.6 \pm 1.0$ cm. The solid Xe is grown on a cold finger made of copper, 2.5 cm in diameter, which is in contact with liquid nitrogen (LN_2). The typical operating temperature is about 68–69 K, obtained by pumping on the LN_2. We found previously that a lower temperature results in a lower background Xe pressure and reduces the attenuation of the metastable atom flux en route to the cold finger.

We used Xe gas (from Linde) with stated purity of 99.99% to grow the layer. The Xe gas flow was continuous in order to maintain a fresh surface uncontaminated by condensible impurities, such as the target gas. The Xe pressure in the detector chamber was typically 2×10^{-4} Torr. The layer of solid Xe is about 1 mm thick or less. It is grown in the field of view of a liquid nitrogen cooled GaAs photomultiplier. The dark count is about $0.5\,s^{-1}$. Provision exists for the placement of filters or a mini-monochromator between the Xe layer and photomultiplier.

TOF spectra were acquired using single photon counting with a time-to-amplitude convertor (TAC) whose output is fed to a pulse height analyser (Nucleus PCA II). The count rates were low enough to avoid TAC pile up. Excitation functions were acquired using gated photon counters (SRI model SR400) and an electron impact energy power supply under the control of a personal computer. Excitation functions from the prompt photons, metastables, and the background were recorded simultaneously.

The operation of the Xe layer detector has been explained earlier, but a quick summary goes as follows. $O(^1S)$ atoms penetrate the solid Xe, thermalize, and form excimers within a few microseconds. The XeO^* state which is formed following thermalization has a radiative lifetime of about 100 ns (Lawrence and Apkarian 1992). The resulting emission occurs in two fairly broad bands, at 725 and 375 nm respectively in order of decreasing intensity. These can be seen in figure 1. We have also observed a very weak emission in the green at about 550 nm which cannot be seen in figure 1, and this is thought to be a surface effect (LeClair and McConkey 1993). The thermalization time and radiative lifetime of the XeO^* excimer is short enough to enable the use of solid Xe as a detector in time-of-flight experiments. Put another way, this detection method effectively shortens the lifetime of $O(^1S)$ so that the emission can be conveniently observed by a photomultiplier.

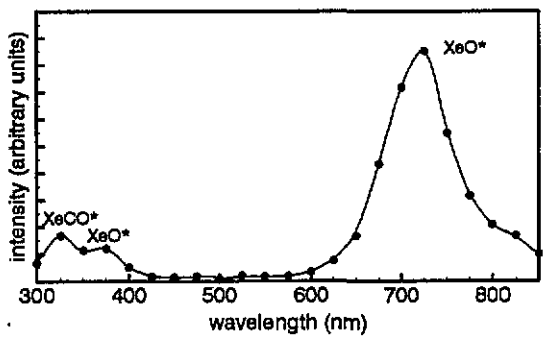

Figure 1. Low resolution spectrum (20 nm bandpass) of fluorescence from the Xe layer following the arrival of neutral metastable fragments in the range 50–500 μs following the impact of a 40 μs wide pulse of electrons on CO_2. The bright feature at 725 nm and the weaker one at 375 nm are due to the arrival of O(^{1}S) atoms, and the feature at 325 nm comes from CO(a $^3\Pi$). The spectrum has not been corrected for variations in sensitivity of the monochromator-photomultiplier combination.

A newly discovered feature of this detection method is its sensitivity to CO(a $^3\Pi$) fragments. Their arrival at the Xe layer produces an emission band in the UV which begins at 350 nm and has a lower limit which lies out of the range of our monochromator (see figure 1). The emission of CO(a $^3\Pi$) in solid rare gases has been reported earlier (Bahrdt *et al* 1987). They irradiated solid rare gas:CO mixtures with monochromatic synchrotron radiation, recording absorption and emission spectra, as well as lifetimes of the emissions. For Xe:CO, the emission of CO(a $^3\Pi$) consists of a continuum lying between 250 and 350 nm, reaching a maximum at about 280 nm. The emission has a lifetime of 19 μs.

3. Results and discussion

3.1. Time-of-flight spectra for O(^{1}S)

TOF spectra for O(^{1}S) fragments produced by EID of CO_2 are shown in figure 2 for various electron impact energies. CO_2 with a stated purity of 99.99% was used. A red filter (Corion LG-595) was in place which limited the wavelength of the detected photons to 600–900 nm. Similar TOF spectra were obtained when a monochromator was used to specify wavelength intervals of 25 nm within that same range. No further TOF structures were observed beyond 250 μs in the 350–900 nm range. The impact energy was calibrated by observing the threshold for CO(a $^3\Pi$) fragments arising from dissociative excitation of CO_2 (see section 3.5). The energies are only accurate to ± 2 eV. Ninety minutes of data acquisition time was used in each case.

Our argument for identifying the TOF structure with the arrival of O(^{1}S) at the Xe layer goes as follows. In the past, it was only possible to record TOF spectra of O(^{5}S), O(R) and CO(a $^3\Pi$) fragments following EID of CO_2 (Allcock and McConkey 1976, Misakian *et al* 1975, Wells *et al* 1972, Freund 1971). These are entirely different in shape from the TOF spectra of figures 2 and 3, so those fragments can be ruled out as being responsible. The short lived, high lying 10 eV state of CO can be eliminated as well since it was not reported in the electron impact dissociation study of CO_2 by Barnett *et al* (1992) who would have been able to see it with their apparatus. The

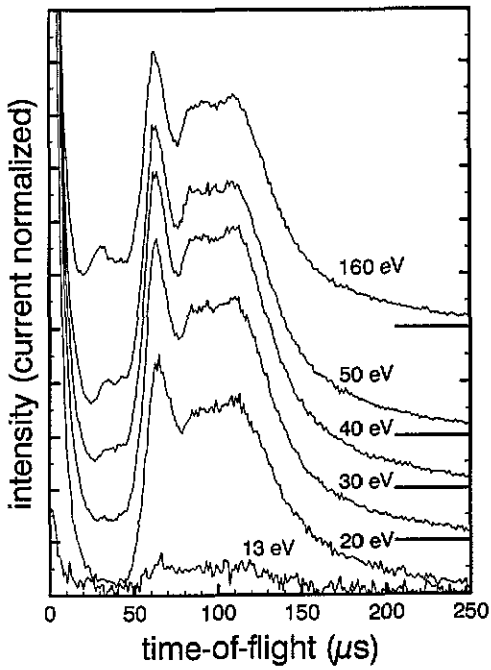

Figure 2. Time-of-flight spectra for $O(^1S)$ atoms following electron impact dissociation of CO_2 for various impact energies with the red filter in place. The spectra at higher energies have been displaced upwards for clarity. In each case the electron beam was pulsed on for 2.5 μs at 2.0 kHz and the source pressure was 9.8 Torr. The resulting integrated current varied from 2 μA at 13 eV to 9 μA to 30 eV and remained constant at higher energies. Each spectrum has been current normalized, and the vertical scales are comparable.

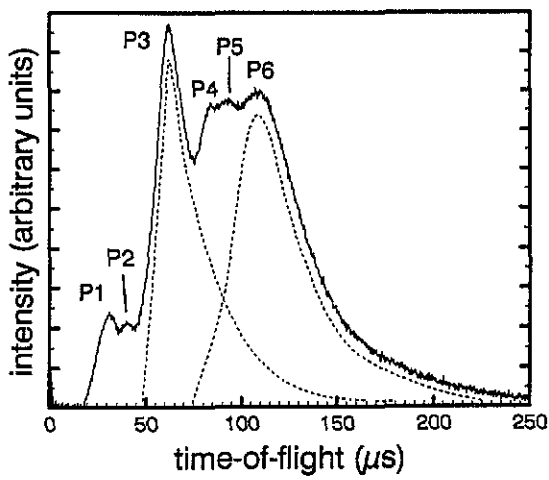

Figure 3. Time-of-flight spectrum for $O(^1S)$ at 100 eV impact energy acquired over 120 h at high resolution. The prompt photon signal and background have been subtracted. The broken lines are explained in the text.

structures could not possibly be produced by the arrival of carbon atoms at the Xe layer, because complete dissociation of the components of CO_2 requires at least 16.5 eV, well above the threshold for the fragments observed here. In addition, metastable C would not produce the same emission spectrum as O(^{1}S) in a Xe matrix.

Conclusive proof, that the fragments being observed are O(^{1}S), comes from a comparison of the spectrum in figure 1 with the previously reported spectra for O(^{1}S) in solid Xe (LeClair and McConkey 1993, LeClair *et al* 1992, Lawrence and Apkarian 1992). TOF spectra identical to those in figures 2 and 3 were obtained by using a filter to observe the weaker 375 nm emissions, and the still weaker emissions at 550 nm, but with poorer statistical significance. It has also been demonstrated that no other long lived state of atomic oxygen (such as O(^{1}D)) produces a TOF spectrum in the 200 to 850 nm range of our photomultiplier.

Figure 3 depicts a single high resolution TOF spectrum taken at 100 eV impact energy using 1 μs pulses at 2.0 kHz, and 120 h of data acquisition. The prompt photon signal has been subtracted. Figure 3 clearly shows that there are six maxima, due to six overlapping structures in the TOF spectrum. Their peaks have been labelled P1 to P6 in order of arrival time, with their maxima at 36, 40, 62, 83, 90 and 107 μs respectively. Without further information it is impossible to deconvolute the TOF spectra and determine the shape of each individual structure. However, we have drawn broken lines which qualitatively represent the structures responsible for P3 and P6. Our argument for this will be presented in section 3.3 where we consider the different channels contributing to O(^{1}S) production.

According to figure 2, structures P1 and P2 appear to have their threshold between 30 and 40 eV. It is possible that the threshold is at a lower energy, but the weak intensity of P1 and P2 made this difficult to determine. The dissociation channels responsible are very energetic; the 20–45 μs region on the TOF scale corresponds to a released kinetic energy of 5–23 eV, assuming CO is the undetected fragment with no vibrational or rotational excitation. The upper limit of this range is probably higher because of the conversion time of the Xe layer.

Structures P3–P6 make up the most prominent feature of the TOF spectrum. Peaks P4, P5 and P6 appear together at threshold (within our energy resolution), and maintain the same intensity ratio at higher impact energies. The threshold was determined to be 11.0 ± 0.5 eV (see the next section). P3 begins to grow at about 12 eV (next section), and quickly rises past P4, P5 and P6. It remains at approximately the same intensity relative to P4 and P5 at higher energies.

Figure 4 shows the released kinetic energy (RKE) spectrum obtained from figure 3 for O(^{1}S) in the 0–5 eV range. P6 appears to dominate the spectrum, P4–P5 appear to be shoulders to P6, and P3 is fairly intense and distinct from the others. P1 and P2 are not shown because their intensities are very weak and RKE distributions very broad. There is an uncertainty in the RKE scale of figure 4 of about $\pm 9\%$ at 2.3 eV due to the spread in arrival time caused by the electron pulse width, size of the interaction volume, and tilt of Xe layer. There would also be a shift of the peaks to higher energies by about 7% if a thermalization time of 3 μs is included. The thermalization time will be smaller at longer arrival times, so the shift should be smaller at lower kinetic energies. Note that a five point average has been applied to the data below 0.5 eV in order to smooth out the large scatter in the points which arises from the t^3 factor in the transformation and the scatter in the data at large flight times.

We have also monitored the signal variation with source pressure and electron beam current at 100 eV. The O(^{1}S) count rate exhibited a linear dependence for up to 2.0 mA

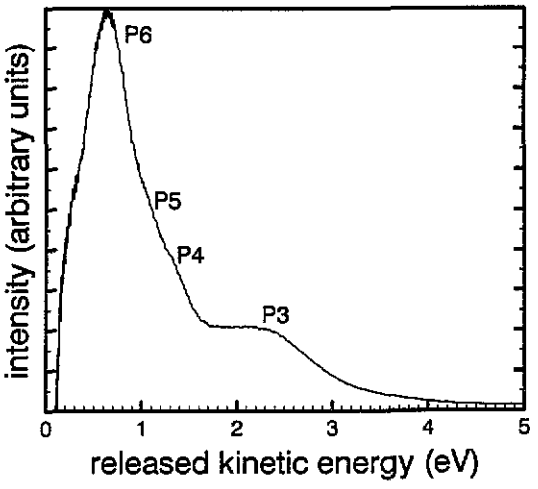

Figure 4. Released kinetic energy transform of the TOF spectrum in figure 3. A 5 point average has been applied to the data below 0.5 eV to smooth the curve.

of equivalent direct current, indicating the absence of secondary processes in the production of $O(^1S)$. The TOF spectral structure showed no dependence on current. The signal versus source pressure exhibited a small quadratic behaviour probably due to the changing flow conditions at the orifice.

3.2. Excitation functions for $O(^1S)$

Figure 5 shows a background subtracted excitation function for the production of $O(^1S)$ in peaks P3–P6 in the 8–20 eV electron impact energy range. Low electron beam currents

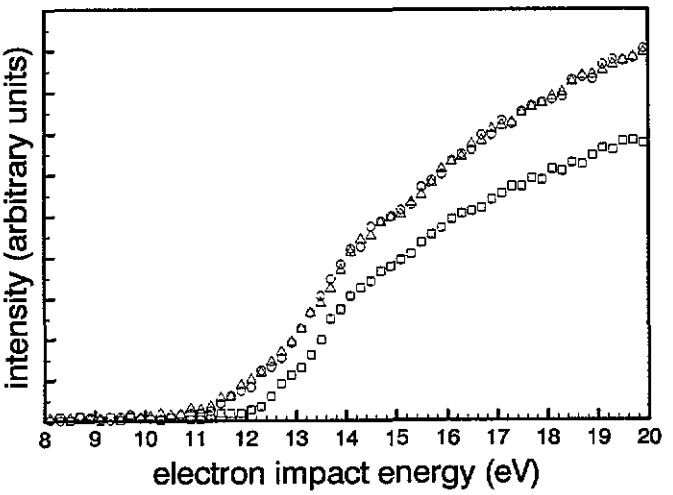

Figure 5. Threshold excitation function for $O(^1S)$ in the 50–75 μs (squares), 75–100 μs (circles) and 100–150 μs (triangles) ranges corresponding to structures P3, P4–P5 and P6 respectively. The data for the latter two ranges have been normalized to one another. The pulse rate was 2.0 kHz, with an integrated electron beam current of 1.60 μA, and the red filter (LG-595) was in place.

were used in order to obtain a constant current over this energy range. However, this necessitated the use of wider electron pulses (10 μs) in order to improve the counting statistics, at the expense of timing resolution. O(^{1}S) production was monitored in three different production channels by setting gates over the intervals 50–75, 75–100 and 100–150 μs for the channels corresponding to P3, P4–P5 and P6 respectively (figure 3). The background was obtained from a counter gated from 300 to 500 μs. The background remained flat throughout the energy range.

Referring to figure 5, production of O(^{1}S) via the channels that produce P4, P5 and P6 begins at 11.0 ± 0.5 eV. It was impossible to determine a difference between channels P4–P5 and P6 within the energy resolution of our electron beam. Both channels closely follow one another, and both have the same slight bump at about 14 eV. The channel responsible for P3 has a threshold about 1.0 eV higher than P4, P5 and P6, and also has a slight bump. The shape for each excitation curve is nearly identical at higher

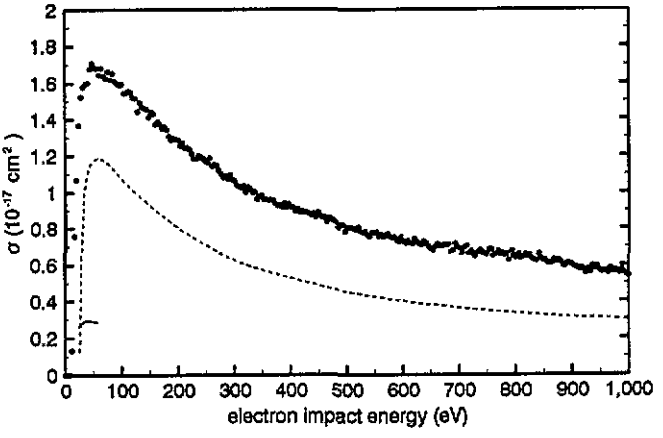

Figure 6. Absolute cross section for O(^{1}S) production following electron impact on CO_2 via all channels. The calibration procedure is discussed in the text. The electron pulse was 30 μs wide, and the gate was 400 μs long and began 20 μs after the pulse was shut off. Some contribution from P1 and P2 was left out by this arrangement to avoid contamination from the prompt photon decay, but it is negligible. Also shown are the cross sections for electron impact excitation of the $1\,^1\Sigma_u^+$ state of CO_2 calculated by Strickland and Green (1969) (broken curve) and Mu-Tao and McKoy (1983) (full curve).

energies, rising from threshold to a very flat maximum between 40 and 70 eV (figure 6), with the maxima shifted slightly towards higher impact energies for the more energetic channels. This behaviour is indicative of electron impact excitation of optically allowed transitions in the parent molecule for channels P3–P6. The slight bumps could indicate a small contribution from a spin-flip transition which requires an electron exchange, and would peak close to threshold.

Figure 6 shows a current normalized 0–1000 eV excitation function for the production of O(^{1}S) from all channels. Absolute calibration of the excitation curve was made using O(^{1}S) from N_2O as a standard. See LeClair and McConkey (1993) for details.

For O(^{1}S) production from CO_2, the relative flow technique was greatly simplified since CO_2 and N_2O have the same mass, and so, to a good approximation, the same source pressure will result in the same gas density in the interaction region. After normalizing for differences in current, O(^{1}S) production from CO_2 was found to be 77.5 ± 2% of that for N_2O at 100 eV. We repeated the comparison at several different

source pressures from 1.0 to 10.0 Torr and found no significant change in the ratio. This indicates that any quenching of $O(^1S)$ atoms that might take place by collisions with the background gas is negligible.

We note that this method assumes the same detection efficiency for $O(^1S)$ by the Xe layer regardless of which gas is present in the background. We found that the ratio was consistently higher by a few per cent after the first exchange of gases took place, but afterwards remained constant. This appears to indicate that the target gases have some transient effect on the surface, since both are condensible.

We also note that this method assumes there is no dependence of the detection efficiency on the velocity of $O(^1S)$ atoms. This is a reasonable assumption since most of the $O(^1S)$ atoms from either N_2O or CO_2 targets travel with similar velocities towards the Xe layer (see LeClair and McConkey 1993). However, there are more slower $O(^1S)$ atoms from CO_2 and they may be less effective in penetrating the Xe matrix and thus be detected with a smaller quantum efficiency. In that case the cross section data given will represent lower limits to the actual values.

Since the cross section for $O(^1S)$ production following 100 eV impact on N_2O was measured to be 2.01×10^{-17} cm^2 ($\pm 10\%$), this places the cross section for $O(^1S)$ production from CO_2 at 1.56×10^{-17} cm^2. The rest of the curve in figure 6 was normalized to this value. The overall uncertainty (12%) comes from our uncertainty in the measurement for N_2O and from our estimated uncertainty in the relative production rate of $O(^1S)$ from CO_2 (see earlier discussion). The integral cross sections for $O(^1S)$ production from EID of CO_2 have been tabulated in table 1 for various energies by drawing a smooth curve through the data of figures 5 and 6. Note that we have assumed that the emission of $O(^1S)$ following dissociation occurs isotropically. While this is generally the case at electron impact energies well above the threshold, there can be marked anisotropies near threshold (Dunn 1962, Misakian *et al* 1975).

Also shown in figure 6 is the semi-empirical calculation by Strickland and Green (1969) which was based on an earlier electron scattering measurement of the optical

Table 1. Absolute integral cross section for $O(^1S)$ production from all channels following electron impact dissociation of CO_2. The uncertainty is $\pm 12\%$.

E (eV)	σ (10^{-17} cm^2)	E (eV)	σ (10^{-17} cm^2)
11	threshold	100	1.56
12	0.20	120	1.50
14	0.51	140	1.44
16	0.82	160	1.38
18	1.03	180	1.32
20	1.22	200	1.27
24	1.46	250	1.15
28	1.54	300	1.04
32	1.60	350	0.96
36	1.64	400	0.91
40	1.67	450	0.85
45	1.68	500	0.80
50	1.69	600	0.72
60	1.68	700	0.65
70	1.65	800	0.61
80	1.63	900	0.57
90	1.60	1000	0.54

oscillator strength, f, for the $X\ ^1\Sigma_g^+ \rightarrow 1\ ^1\Sigma_u^+$ (11.0 eV) transition which is known to produce $O(^1S)$. They used $f = 0.12$ from Lassettre and Shiloff (1965) (later remeasured at 0.12 ± 0.01, Klump and Lassettre 1978) which is in excellent agreement with the photoabsorption result for the same transition, measured at 0.12 by Inn and Zelikoff (1953). Our cross section measurement is much larger and shows that the contributions from other channels are significant, see next section.

The original calculation for the $O(^1S)$ production cross section by Strickland and Green was increased by a factor of 2.5 by McConnell and McElroy (1970) because Strickland and Green's calculation for $CO(a\ ^3\Pi)$ production was less by a factor of 2.5 than experimental measurements available at the time. This was due to cascade contributions to $CO(a\ ^3\Pi)$ production which the experiment was able to measure (Freund and Klemperer 1967) and Strickland and Green could not take into account. This modification was still accepted later (Fox and Dalgarno 1979). However, using the factor of 2.5 appears unjustified, especially since not all of the production channels for $O(^1S)$ from electron impact on CO_2 were known. The only cascade contribution, $O(3s''\ ^1P^\circ \rightarrow\ ^1S,\ \lambda = 121.8\ nm)$ is very small, with an electron impact cross section for CO_2 of $5.43 \times 10^{-20}\ cm^2$ at 200 eV incident energy (Kanik *et al* 1992), and they may not all be accompanied by $CO(a\ ^3\Pi)$ production.

More recently, we note that the integral cross section for electron impact excitation the $^1\Sigma_u^+$ state of CO_2 has been calculated by Mu-Tao and McKoy (1983). It reaches a value of about $0.3 \times 10^{-17}\ cm^2$ at 40 eV, and is also shown in figure 6. This is consistent with our interpretation that other channels are making significant contributions to $O(^1S)$ production.

3.3. Identification of the parent molecular state(s) responsible for $O(^1S)$ production

The ground state of CO_2 is $X\ ^1\Sigma_g^+$ and correlates to $CO(^1\Sigma^+)$ and $O(^1D)$ at the dissociation limit which lies at 7.42 eV above the ground vibrational state of CO_2. Several other dissociation limits are listed in table 2 (Herzberg 1967, Huber and Herzberg 1979).

Table 2. Dissociation limits (in eV) for various products from CO_2.

$CO(^1\Sigma^+) + O(^3P)$	5.45	$CO(a\ ^3\Pi) + O(^1D)$	13.46
$CO(^1\Sigma^+) + O(^1D)$	7.42	$CO(^1\Sigma^+) + O(^5S^\circ)$	14.60
$CO(^1\Sigma^+) + O(^1S)$	9.64	$CO(a\ ^3\Pi) + O(^1S)$	15.68
$CO(a\ ^3\Pi) + O(^3P)$	11.49	$CO(b\ ^3\Sigma^+) + O(^3P)$	15.84
$CO(a'\ ^3\Sigma^+) + O(^3P)$	12.31	$C(^3P) + O(^3P) + O(^3P)$	16.54
$CO(d\ ^3\Delta) + O(^3P)$	12.97		

By inspection of the table, structures P3–P6 come from a dissociation of CO_2 which produces $CO(^1\Sigma^+) + O(^1S)$, since the thresholds for these structures lie well below the minimum 15.68 eV threshold required for the next possible $O(^1S)$ channel. According to the Wigner–Witmer rules, $CO(^1\Sigma^+) + O(^1S)$ correlates to one state of CO_2 only, designated $1\ ^1\Sigma_u^+$. Thus it is accessible from the ground state by a dipole and spin allowed transition. This transition has been identified with the intense feature at 11.0 eV in photo-absorption spectra (Koyano *et al* 1975) and electron energy loss (EEL) spectra (Hubin-Franskin *et al* 1988).

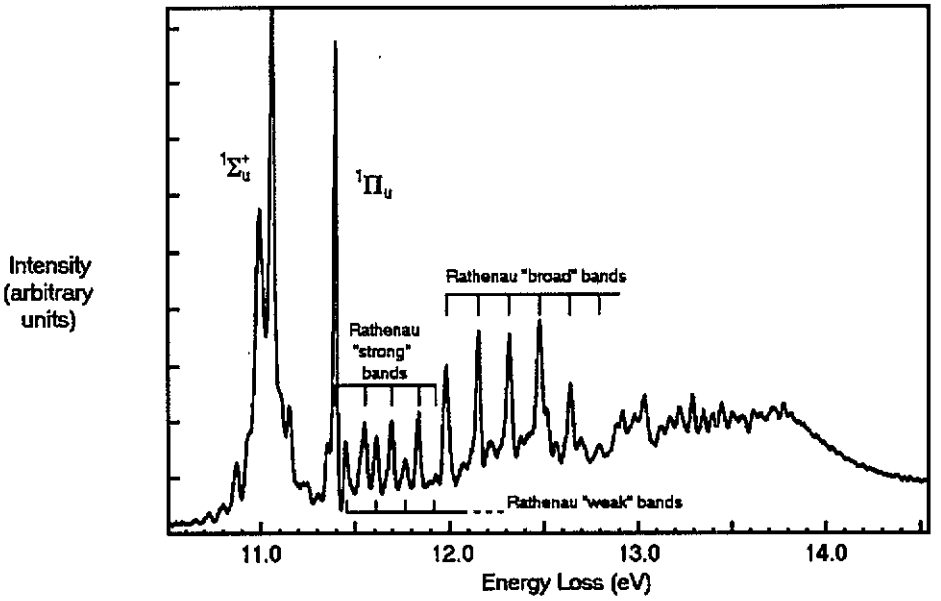

Figure 7. Deconvoluted electron energy loss spectrum for CO_2 taken from Hubin-Franskin *et al* (1988). The incident energy was 60 eV, and the scattered electrons were collected at 4° from the incident beam.

An EEL spectrum taken from Hubin-Franskin *et al*, figure 7, shows the 11.0 eV feature and many others in the 10.5 to 14.5 eV region. The multi-peaked structure of the 11.0 eV feature has been dificult to explain. The recent accurate *ab initio* calculations of the potential surfaces of the excited states of CO_2 by Spielfiedel *et al* (1993) has led these authors to conclude that it is due to complex avoided crossings and vibronic coupling effects between the Rydberg and valence $^1\Sigma_u^+$ states in the Franck–Condon region.

Regardless of its structure, it is clear from the width of the 11.0 eV feature and the 9.64 eV dissociation limit that the RKE distribution of the dissociation products from the $^1\Sigma_u^+$ surface will span a range of about 1.2 to 1.6 eV, with a maximum at about 1.4 eV, assuming there is no vibrational or rotational motion of the CO fragment. According to the work of Spielfiedel *et al* (1993) the $CO_2(1\,^1\Sigma_u^+)$ state is bound along the symmetric stretch coordinate in the Franck–Condon region. However this barrier to dissociation should vanish or dramatically decrease when the molecule is bent (Chambaud 1994). Thus the CO fragment will be vibrationally and rotationally excited as the molecule dissociates (Herzberg 1967). This will shift the observed RKE distribution to lower energies. It is unlikely that the structure of the 11.0 eV feature as seen in the EEL spectra (or the more detailed structure from photo-absorption spectra) would show up in the RKE distribution.

Since the $1\,^1\Sigma_u^+$ surface is the first accessible O(^{1}S) production channel, the RKE of this channel will be the lowest of those we observe at impact energies below 15.68 eV, the threshold for the next channel (table 2). For this reason, we identify the maximum at P6, which appears at 11.0 eV and remains at higher impact energies, as belonging to a TOF structure which arises directly from the $1\,^1\Sigma_u^+$ surface. P6 has a maximum at 0.7 eV in the RKE distribution of figure 4. This would imply that roughly 0.8 eV of

energy is taken up by the vibrational and rotational excitation of the undetected CO fragment.

Also, if P6 arises from the excitation to the $1\ ^1\Sigma_u^+$ state, then, using the EEL spectrum of figure 7, the predicted maximum RKE for P6 is 1.6 eV. This corresponds to a TOF of about 75 μs in figure 3. This would mean that P6 is the tip of a structure with a very broad base, which we have sketched qualitatively in figure 3. In addition this implies that the structures giving rise to P4 and P5 have relatively smaller intensities, which appears to be the case in the RKE spectrum (figure 4).

Further information can be gleaned from photodissociation experiments on CO_2 performed in the 1970s. Koyano *et al* (1975) monitored $O(^1S)$ production versus wavelength in a photodissociation study of CO_2 and found that it closely followed the complex photoabsorption spectrum from 10.68 to 11.29 eV. This range was extended by Slanger *et al* (1977) who made quantum yield measurements for $O(^1S)$ up to 11.68 eV, where it was about 50%. Up to that point the quantum yield was nearly flat at about 100%, except for a dip to about 20% at 11.38 eV, the position of the second most intense feature ($^1\Pi_u$) in figure 7. No further observations of $O(^1S)$ production past 11.68 eV were possible due to instrumental limitations.

The fact that $O(^1S)$ production is still taking place at 11.68 eV, which is well removed from the 11.0 eV structure (figure 7) and into the region of the Rathenau 'strong' and 'weak' vibrational progressions, indicates that pre-dissociation to the $1\ ^1\Sigma_u^+$ surface is probably occurring. All of the Rathenau bands are known to pre-dissociate (Cossart-Magos *et al* 1988). State assignments of the features in this energy region are somewhat complicated. Hubin-Franskin *et al* (1988) indicate that all of the Rathenau bands behave like optically allowed transitions, but they have found evidence for some states interspersed among those bands which arise from symmetry forbidden transitions from the ground state. The calculations of Werner *et al* (1990) suggest that some of the transitions in the region of the Rathenau 'strong' and 'weak' bands may be to triplet states.

Because of the low intensity of the features in the 11.5–12.0 eV region of the EEL spectrum (figure 7), we have assigned the structures P4 and P5 as coming from pre-dissociation of the excited states responsible for those features. P4 and P5 have maxima in the TOF spectrum which correspond to a RKE of roughly 1.2 and 1.3 eV respectively. If the average excitation energy of the undetected CO fragment was 0.8 eV, as it was with P6, this would place the threshold for P4 and P5 in the region of the Rathenau strong and weak bands. According to our interpretation, the reason why we do not see this threshold clearly in figure 5 is due to contamination from the strong channel which produces P6. Since P4 and P5 remain at the same intensity with respect to the others at high energies (figure 2) they must also arise from optically allowed transitions. The slight bump at 14 eV in the near threshold excitation function of figure 5 may be due to transitions from the singlet ground state to triplet states, but pre-dissociation from pure triplet states to singlet states is forbidden, so the mechanism is unclear.

Comparison of the strengh of P3 in our RKE spectrum (figure 4) with the EEL spectrum of figure 7, and its threshold of around 12.0 eV (figure 5), leads us to conclude that the $O(^1S)$ channels giving rise to P3 comes from pre-dissociation of the excited states responsible for the Rathenau 'broad' bands to the $1\ ^1\Sigma_u^+$ surface. We have sketched the possible structure responsible for P3 in figure 3. The Rathenau 'broad' bands are a single vibrational progression belonging to a single electronic state (McDiarmid and Doering 1984). Werner *et al* (1990) have designated the state $^1\Pi_u$. Thus the selection rules for pre-dissociative transitions are satisfied (Herzberg 1967).

Further support for this conclusion comes from a calculation of the optical oscillator strength from the cross section of $O(^1S)$ production in figure 6. From the Bethe–Born approximation (Inokuti 1971), the cross section, σ_i, for electron impact excitation of the ith state is given by

$$\sigma_i = \frac{4\pi a_0^2}{E/R}\,\frac{f_i}{E_i/R}\ln(4C_iE/R) \tag{2}$$

where a_0 is the Bohr radius, R the Rydberg constant, E is the electron impact energy, E_i is the transition energy of the ith state, C_i is a constant dependent on that transition and f_i is the optical oscillator strength for the same. Using (2) we have calculated an optical oscillator strength of $f_0 = 0.38 \pm 0.05$ from the data in figure 6. The large error comes from using an average transition energy, E_i, of 12.4 eV. This would apply for all channels contributing to $O(^1S)$ production from 11.0 eV to 13.77 eV. We note that the maximum RKE of P3 of about 4.5 eV in figure 4 indicates contributions from the pre-dissociation of excited states above the first ionization threshold of CO_2 (13.77 eV), particularly if vibrational excitation of the CO fragment was occurring.

Since $f = 0.12$ for the channel from the 11.0 eV transition, this leaves a $f = 0.26$ for the remaining channels. This can be accounted for if we use $f = 0.20$ for the Rathenau 'broad' bands as measured by Lassettre and Shiloff (1965). The remaining oscillator strength would come from the less intense channels leading to P1, P2, P4 and P5 in the TOF spectra and pre-dissociation from excited states of CO_2 near the ionization threshold.

The very energetic, small structures which we have labelled P1 and P2 remain unidentified. They have a possible threshold around 30 eV. Such high thresholds for electron impact dissociation have been observed before (Misakian *et al* 1975) and could involve ionization or complete fragmentation of the target molecule.

3.4. Time-of-flight spectrum for $CO(a\,^3\Pi)$

Figure 8 shows a further TOF spectrum following electron impact on CO_2. The conditions were similar to those used to acquire the TOF spectra in figure 3, but a longer

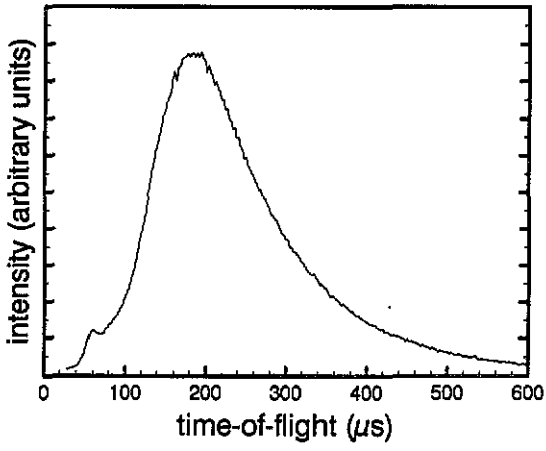

Figure 8. Time-of-flight spectrum for $CO(a\,^3\Pi)$ fragments following electron impact (30 eV) on CO_2. The structure at 60 μs is from $O(^1S)$ (see text).

electron pulse (10 μs) and shorter acquisition time (10 h) was used. The electron impact energy was 30 eV. The solid Xe layer was used as the detector, but this time an ultraviolet filter (Rolyn UG-11) with transmission range from 240 nm to 370 nm was placed between the solid Xe and photomultiplier. The small peak at 60 μs is due to the weak fluorescence band centred around 375 nm caused by O(^{1}S) impacting on the solid Xe (see figure 1). It comes from structure P3 in figure 3. There was virtually no change in TOF structure with higher electron impact energies, so only one TOF spectrum is shown.

There have been several TOF studies of the production of CO(a $^3\Pi$) following electron impact on CO_2 (e.g. see Freund 1971, Wells *et al* 1972). Since the structure of our TOF spectrum is identical to those earlier studies, we conclude that it is caused by the arrival of CO(a $^3\Pi$) fragments at the solid Xe. This would mean that the lifetime of CO(a $^3\Pi$) was being substantially shortened by the solid Xe. The gas phase lifetime of CO(a $^3\Pi$) is dependent on its degree of rotational excitation. Johnson (1972) has measured an average lifetime of 9 ms for CO(a $^3\Pi$) produced by electron impact dissociation of CO_2.

Support for our conclusion comes from the observation of fluorescence from CO(a $^3\Pi$) in solid Xe by Bahrdt *et al* (1987). Our spectrum of emissions from the Xe layer following the arrival of the CO metastable fragments (figure 1) coincides with the emission continuum for CO(a $^3\Pi$) in Xe observed by Bahrdt *et al* (1987), within the range of our monochromator. In addition, we replaced the solid xenon surface with an identical one of clean solid copper (work function = 4.65 eV), in the field of view of a Channeltron electron multiplier in order to detect CO(a $^3\Pi$) by Auger electron emission from the copper (e.g. see Allcock and McConkey 1976). We obtained the same TOF spectrum, with a maximum roughly 25 μs earlier than that in figure 8. This concurs with the 19 μs lifetime of CO(a $^3\Pi$) in solid Xe measured by Bahrdt *et al* (1987). Finally, we have observed TOF spectra with the Xe layer and the UG-11 filter in place following electron impact excitation of CO. Its excitation function has a threshold at 6.0 eV and a maximum at 10 eV, as expected for excitation of CO(a $^3\Pi$) from CO (LeClair *et al* 1994).

3.5. *Excitation function for CO(a $^3\Pi$)*

Figure 9 shows the excitation function for CO(a $^3\Pi$) following electron impact dissociation of CO_2. The conditions were similar to those used to acquire O(^{1}S) excitation functions, only a wider electron pulse (40 μs), slower shot rate (1.0 kHz), and longer gate interval (120–320 μs) were used. The UG-11 filter was in place. The threshold for CO(a $^3\Pi$) production following electron impact on CO_2 has been measured at 11.8 eV (Freund 1971). We used this value to calibrate our energy scale for CO(a $^3\Pi$) and O(^{1}S) excitation functions.

Our excitation function in figure 9 resembles the one obtained by Freund (1971) except that our maximum occurs at about 22 eV, rather than 27 eV. This might be explained by differences in the electron beam uniformity. We draw your attention to three features in figure 9.

There is a slight bump at 14 eV which probably arises from cascade from CO(a' $^3\Sigma^+$) and CO(d $^3\Delta$). These cascades produce the Asundi and Triplet bands with lifetimes of around 5 and 10 μs respectively (van Sprang *et al* 1977). The bump at about 17.5 eV probably comes from cascade from CO(b $^3\Sigma^+$), producing the third positive bands. The (00) and (01) lines of that transition lie at 283.3 and 297.7 nm with a lifetime of 56 ns (van Sprang *et al* 1977). We have observed a threshold of 16.2 eV for prompt photon production using the UG-11 filter. This is probably due to production of the third

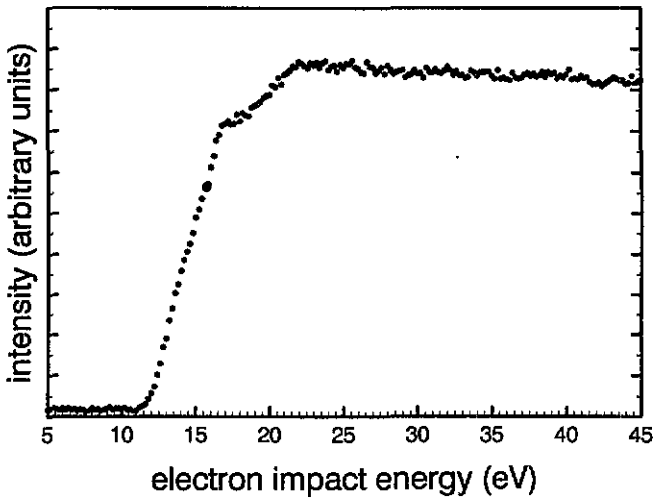

Figure 9. Near threshold excitation function for $CO(a\,^3\Pi)$. The data have been normalized to account for variations in the electron beam current with energy.

positive bands, since the dissociation limit of $CO(b\,^3\Sigma^+) + O(^3P)$ is 15.84 eV. The slight peak at 22 eV may come from another channel in which $O(^5S)$ is produced along with $CO(a\,^3\Pi)$. This channel has been reported earlier by Allcock and McConkey (1976) and Misakian *et al* (1975) and has a threshold at about 20.0 eV.

The rapid rise to maximum of the excitation function for $CO(a\,^3\Pi)$ indicates the prominent role played by a spin-flip transition to the dissociating parent state. However, the slow fall off after the maximum has been reached is typical of optically allowed transitions, so there appear to be contributions from both excited triplet and singlet states of CO_2.

We have not measured the cross section for production of $CO(a\,^3\Pi)$ by electron impact dissociation of CO_2, owing to a lack of means by which to calibrate the sensitivity of the Xe layer to $CO(a\,^3\Pi)$. The most recent measurement of that cross section by Erdman and Zipf (1983) is $2.4 \times 10^{-16}\,cm^2$ at 80 eV. By normalizing our excitation functions to that value, we obtain $2.8 \times 10^{-16}\,cm^2$ at 22 eV. This reduces to $0.76 \times 10^{-16}\,cm^2$ at 1000 eV.

Despite the much larger cross section for $CO(a\,^3\Pi)$ production compared to $O(^1S)$, we did not observe a corresponding increase in the count rate for $CO(a\,^3\Pi)$ over $O(^1S)$ with our apparatus. By comparison of the two count rates under the same conditions, but with different filters, together with our quantum efficiency of 25% for $O(^1S)$ detection by the Xe layer (LeClair and McConkey 1993), the spectral distribution of $CO(a\,^3\Pi)$ in solid Xe (Bahrdt *et al* 1987), and the transmission curves of the filters used, we obtained a quantum efficiency of 0.33% for $CO(a\,^3\Pi)$ detection by solid Xe. We did not take into account any in-flight quenching of $CO(a\,^3\Pi)$ by collisions with background molecules, or any possible velocity dependence of the quantum efficiency. In-flight radiative decay of $CO(a\,^3\Pi)$ is negligible in this case.

4. Conclusions

We have demonstrated the usefulness of a layer of solid Xe as a means to selectively detect the neutral metastable particles $O(^1S)$ and $CO(a\,^3\Pi)$. Selection of either is done

simply by the use of an appropriate filter. The TOF spectra and excitation functions for both species indicate contributions from several different channels. We have been able to associate some of the $O(^1S)$ channels with pre-dissociation from excited states of CO_2, such as those responsible for the intense Rathenau 'broad' bands, and have measured the absolute cross section for $O(^1S)$ production following electron impact dissociation of CO_2 for the first time. It would be interesting to apply this detector to a new photodissociation study of CO_2.

Acknowledgments

We are grateful for financial assistance from the Natural Sciences and Engineering Research Council of Canada, the Donors of the Petroleum Research Fund administered by the American Chemical Society, and NATO, Division of Scientific Affairs. We thank the technical staff of the mechanical and electronic workshops at the University of Windsor for their expert assistance without which this experiment would not have been possible. We thank Arie van Wijngaarden and Frank Holuj for helpful input and loan of equipment, and Michael Brown for assistance. Finally, we wish to thank Gilberte Chambaud and Pavel Rosmus for useful information and their unpublished potential curves of CO_2.

References

Allcock G and McConkey J W 1976 *J. Phys. B: At. Mol. Phys.* **9** 2127
Bahrdt J, Gürtler P and Schwentner N 1987 *J. Chem. Phys.* **86** 6108
Barnett S M, Mason N J and Newell W R 1992 *J. Phys. B: At. Mol. Opt. Phys.* **25** 1307
Chambaud G 1994 Personal communication
Conway R R 1981 *J. Geophys. Res.* **86** 4767
Cossart-Magos C, Jungen M and Launay F 1985 *Mol. Phys.* **61** 1077
Dunn G H 1962 *Phys. Rev. Lett.* **8** 62
Erdman P W and Zipf E C 1983 *Planet. Space Sci.* **31** 317
Fox J L and Dalgarno A 1979 *Planet. Space Sci.* **27** 491
—— 1981 *J. Geophys. Res.* A **86** 629
Freund R S 1971 *J. Chem. Phys.* **55** 3569
Freund R S and Klemperer W 1967 *J. Chem. Phys.* **47** 2897
Herzberg G 1967 *Electronic Spectra of Diatomic Molecules* (Toronto: Van Nostrand Reinhold)
Huber K P and Herzberg G 1979 *Constants of Diatomic Molecules* (Toronto: Van Nostrand Reinhold)
Hubin-Franskin M-J, Delwiche J, LeClerc B and Roy D 1988 *J. Phys. B: At. Mol. Opt. Phys.* **21** 3211
Inn E C Y and Zelikoff M 1953 *J. Chem. Phys.* **21** 1648
Inokuti M 1971 *Rev. Mod. Phys.* **43** 297
Itikawa Y and Ichimura A 1990 *J. Phys. Chem. Ref. Data* **19** 637
Johnson C E 1972 *J. Chem. Phys.* **57** 576
Kanik I, Ajello J M, James G K and Franklin B O 1992 Personal communication
Klump K N and Lassettre E N 1978 *J. Electron Spectros. Relat. Phenom.* **14** 215
Koyano I, Wauchop T S and Welge K H 1975 *J. Chem. Phys.* **63** 110
Lassettre E N and Shiloff J C 1965 *J. Chem. Phys.* **43** 560
Lawrence W G and Apkarian V A 1992 *J. Chem. Phys.* **97** 2229
LeClair L R, Brown M D, McConkey J W 1994 to be published
LeClair L R, Corr J J and McConkey J W 1992 *J. Phys. B: At. Mol. Opt. Phys.* **25** 2647
LeClair L R and McConkey J W 1993 *J. Chem. Phys.* **99** 4566
McConnell J C and McElroy M B 1970 *J. Geophys. Res.* **75** 7290
McDiarmid R and Doering J P 1984 *J. Chem. Phys.* **80** 648
Misakian M, Mumma M J and Faris J F 1975 *J. Chem. Phys.* **62** 3442

Mu-Tao L and McKoy V 1983 *J. Phys. B: At. Mol. Phys.* **16** 657
Slanger T G, Sharpless R L and Black G 1977 *J. Chem. Phys.* **67** 5317
Spielfiedel A, Feautrier N, Chambaud G, Rosmus P and Werner H-J 1993 *Chem. Phys. Lett.* **216** 162
Strickland D J and Green A E S 1969 *J. Geophys. Res.* **74** 6415
van Sprang H A, Möhlmann G R and de Heer F J 1977 *Chem. Phys.* **24** 429
Wells W C, Borst W L and Zipf E C 1972 *J. Geophys. Res.* **77** 69
Werner H-J, Spielfiedel A, Feautrier N, Chambaud G and Rosmus P 1990 *Chem. Phys. Lett.* **175** 203
Zipf E C 1984 *Electron–Molecule Interactions and their Applications* vol 1 ed L G Christophorou (New York: Academic) p 335